Journal of Medicinal Chemistry

Article

pubs.acs.org/jmc

Nitric Oxide (NO) Releasing Poly ADP-ribose Polymerase 1 (PARP-1) Inhibitors Targeted to Glutathione S-Transferase P1-Overexpressing Cancer Cells

Anna E. Maciag,*[,†] Ryan J. Holland,[‡] Youseung Kim,[‡] Vandana Kumari,[§] Christina E. Luthers,[‡] Waheed S. Sehareen,[‡] Debanjan Biswas,[‡] Nicole L. Morris,[∥] Xinhua Ji,[§] Lucy M. Anderson,[‡] Joseph E. Saavedra,[†] and Larry K. Keefer[‡]

[†]Chemical Biology Laboratory, Leidos Biomedical Research, Inc., Frederick National Laboratory for Cancer Research, Frederick, Maryland 21702, United States

[‡]Chemical Biology Laboratory, National Cancer Institute, Frederick, Maryland 21702, United States

[§]Macromolecular Crystallography Laboratory, National Cancer Institute, Frederick, Maryland 21702, United States

[∥]Laboratory Animal Sciences Program, Leidos Biomedical Research, Inc., Frederick National Laboratory for Cancer Research, Frederick, Maryland 21702, United States

Supporting Information

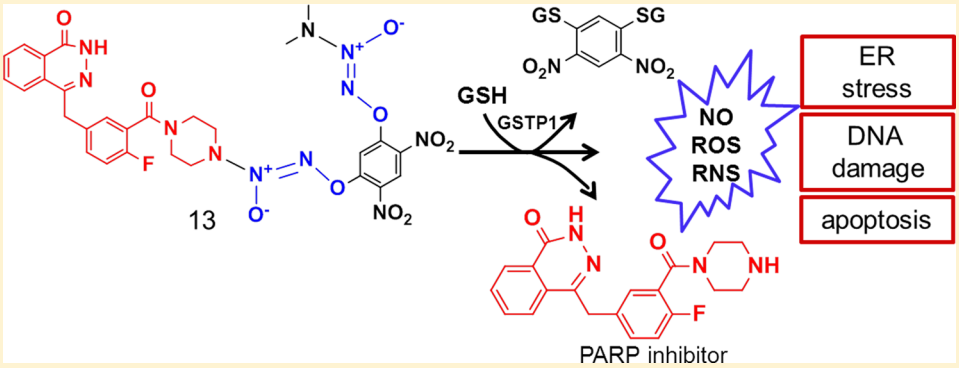

ABSTRACT: We report the antitumor effects of nitric oxide (NO) releasing derivatives of the PARP-1 inhibitor olaparib (**1**). Compound **5b** was prepared by coupling the carboxyl group of **3b** and the free amino group of arylated diazeniumdiolated piperazine **4**. Analogue **5a** has the same structure except that the F is replaced by H. Compound **13** is the same as **5b** except that a $Me_2N–N(O)=NO–$ group was added para and ortho to the nitro groups of the dinitrophenyl ring. The resulting prodrugs are activated by glutathione in a reaction accelerated by glutathione S-transferase P1 (GSTP1), an enzyme frequently overexpressed in cancers. This metabolism generates NO plus a PARP-1 inhibitor simultaneously, consuming reducing equivalents, leading to DNA damage concomitant with inhibition of DNA repair, and in the case of **13** inducing cross-linking glutathionylation of proteins. Compounds **5b** and **13** reduced the growth rates of A549 human lung adenocarcinoma xenografts with no evidence of systemic toxicity.

INTRODUCTION

Poly ADP-ribose polymerase 1 (PARP-1) is a critical enzyme in the repair of DNA strand breaks. This 116 kDa nuclear protein detects DNA single strand breaks and utilizes NAD^+ as a substrate to poly(ADP-ribosyl)ate nuclear proteins, resulting in relaxation of chromatin and recruitment of other repair proteins to the damaged site. PARP-1 is an attractive antitumor target because of this vital role in DNA repair. The current clinical approaches to the development of PARP-1 inhibitors include either (1) the utilization as a single agent in BRCA1 or BRCA2-deficient cancers where inhibition of PARP results in synthetic lethality or (2) the utilization in combination with DNA damaging therapeutics (radiation or chemotherapy) to increase maximum therapeutic benefit of these agents by blocking the repair process. There are multiple ongoing clinical trials evaluating the efficacy of PARP-1 inhibitors as chemopotentiators in several cancers, including non-small-cell lung cancer (NSCLC). However, early phase clinical studies of PARP-1 inhibitor, compound **1**, in combination with topotecan,[1] dacarbazine,[2] or cisplatin plus gemcitabine[3] showed dose-limiting toxicity that was more pronounced than that seen with the chemotherapeutic agents alone. Therefore, targeted

Received: October 4, 2013
Published: February 12, 2014

delivery of PARP inhibitors selectively to cancer cells could be a solution to overcome these systemic toxicity problems.

Diazeniumdiolate-based nitric oxide (NO) releasing prodrugs developed in our laboratory have proven to be effective as anticancer agents in a number of in vitro and in vivo models.[4−9] The lead compound, O^2-(2,4-dinitrophenyl) 1-[(4-ethoxycarbonyl)piperazin-1-yl]diazen-1-ium-1,2-diolate (JS-K, **2**), exhibits a multifaceted mechanism of action initiated by depletion of intracellular GSH and induction of oxidative stress, followed by the activation of stress signaling, abrogated mitochondria function, DNA damage, and apoptosis. DNA single strand break damage (measured by Comet assay) was observed in the H1703 NSCLC cell line after a 1 h treatment with **2**, and massive DNA damage was seen after 24 h. In multiple myeloma cells, **2** caused DNA double strand break damage.[6] We hypothesized that inhibition of PARP may enhance the potency of **2** and other NO-releasing prodrugs of the arylated diazeniumdiolate class.

In this work, we have designed and synthesized NO-releasing PARP-1-inhibitor prodrugs that are activated by reaction with glutathione (GSH), a reaction that is accelerated by glutathione S-transferase (GST), a family of phase II detoxification enzymes. We show that these hybrid prodrugs are effective against cancer cells in vitro and in vivo. Activation of the compounds by GSTP1, an isoform of GST that is frequently overexpressed in cancers, should result in the preferential metabolism and thus release of cytotoxins in cancer cells, potentially diminishing systemic toxicity associated with PARP inhibition.

RESULTS AND DISCUSSION

Prodrug Design Considerations. Our specific strategy here is to combine the structural features of the established PARP-1 inhibitor **1** and arylated diazeniumdiolate **2**, structures shown in Scheme 1. Specifically, we wanted to produce

Scheme 1. Structures of the PARP-1 Inhibitor 1 and Anticancer Drug Candidate 2[a]

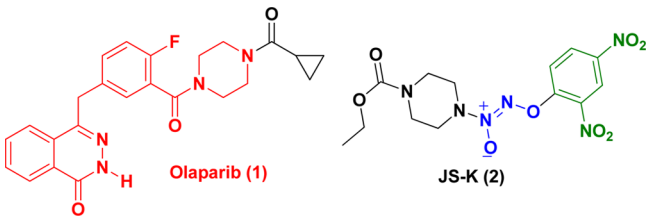

[a]Structural features to be merged in designing NO-releasing PARP inhibitors for the present study are color coded: green for the arylating fragment that is transferred to GSH in the activation step; red for the PARP inhibitor moiety; and blue for the two molecules of cytolytic nitric oxide released on activation.

molecules that link the PARP-inhibitory skeleton of **1** (the red portion of structure **1** in Scheme 1; the black cyclopropane carboxamide group is not necessary for PARP-1 inhibition) with the electrophilic aryl ring shown in green and the caged NO molecules shown in blue in Scheme 1. Accordingly, we reacted known compounds **3a** and **3b**[10] with **4**[7] to obtain the first two drug candidates, **5a** and **5b**, as shown in Scheme 2. Our hypothesis was that attack by GSH on these molecules would lead to consumption of a reducing equivalent through irreversible arylation of the GSH, with simultaneous generation of two NOs plus known PARP inhibitors **6a** and **6b**, as illustrated in Scheme 3.

Prodrug Activation and NO Release. The first step in the activation of these prodrugs is the arylation of GSH, liberating a diazeniumdiolate ion that spontaneously decomposes to NO, freeing the PARP-inhibitory part of the molecule. Accordingly, **5a** and **5b** reacted smoothly with GSH to generate the expected products, shown in Scheme 3. The rates of reaction of **5a** and **5b** with 4 mM GSH in aqueous pH 7.4 phosphate buffer (0.1 M) containing 50 μM diethylenetriaminepentaacetic acid at 37 °C were determined. The $t_{1/2}$ for **5a** was 11.2 min, and the $t_{1/2}$ for **5b** was 11.6 min. Liquid chromatography/mass spectrometry (LC/MS) analysis of the reaction mixture after 2 half-lives confirmed that 25% of the parent compound was still present while 75% consisted of deacylated compound **1** (**6b**) and the aryl-glutathione conjugate (**7**) (Scheme 3, Figure S1).

PARP-1 Enzyme Inhibition. The ability of the new compounds to inhibit PARP-1 enzymatic activity was tested using an assay that measures incorporation of biotinylated poly ADP-ribose onto histone proteins. **5a** and **5b** were compared to **1** and authentic compounds **6a** and **6b** that are products of **5a** and **5b** activation (Scheme 3). Compounds **6a** and **6b** had PARP-1 inhibitory activities comparable to that of **1**. PARP-1 enzyme IC_{50} values estimated for **6a**, **6b**, and **1** were 30.5, 6.9, and 15.5 nM, respectively (Figure 1). Both prodrugs **5a** and **5b**, without activation by GSH, were less potent, with IC_{50} of 123 nM for **5a** and 58 nM for **5b**.

In Vitro Antiproliferative Activity. Compounds **5a** and **5b** inhibited proliferation of an extensive panel of NSCLC cell lines with IC_{50} concentrations ranging from 3 to 20 μM (Table 1). IC_{50} values for NO-releasing PARP-1 inhibitor prodrugs were significantly lower than those of **1** for the most sensitive cell lines.

The IC_{50} values correlated with endogenous ROS levels and with levels of antioxidant enzyme peroxiredoxin 1 and DNA repair enzyme 8-oxoguanine DNA glycosylase (OGG1, Figure S2). Depleting the cell's GSH during prodrug activation combined with NO release led to induction of oxidative/nitrosative stress (Figure S3) and cytotoxicity through cellular stress overload, especially in cells with high endogenous ROS levels. Since the proliferation screen and measurements of PARP-1 inhibitory activities of both prodrugs showed fluoro-substituted analogue **5b** to be more potent than **5a**, we decided to focus on **5b** for further development.

DNA Damage and Activation of Apoptosis. Activation of PARP is an ATP-depleting process. Cellular levels of ATP fall below a critical level, and cells with substantial DNA damage cannot enter apoptosis, rendering them resistant to this form of cell death or susceptible to necrosis. Therefore, inhibition of PARP-1 in combination with substantial DNA damage would conserve cellular energy and could allow tumor cells to undergo apoptosis in response to DNA-damaging NO, eliminating toxic effects or immune responses associated with necrosis.

Twenty-four-hour treatment with NO-releasing PARP-1 inhibitor prodrug **5b** resulted in significant DNA strand break damage as observed by Comet assay. Treatment with **5b** at 5 μM resulted in a stronger Comet signal, compared with 20 μM **1** (Figure 2A). A strong apoptotic signal (as evidenced by cleaved caspase 7) was seen in cells treated with **5b**, while the same concentration of **1** did not trigger apoptosis (Figure 2B).

Cellular Uptake and GST-Catalyzed Metabolism. To validate the release of the PARP-1 inhibitor in cells, we

dx.doi.org/10.1021/jm401550d | J. Med. Chem. 2014, 57, 2292−2302

Scheme 2. Synthesis of NO-Releasing PARP-1 Inhibitors 5a and 5b

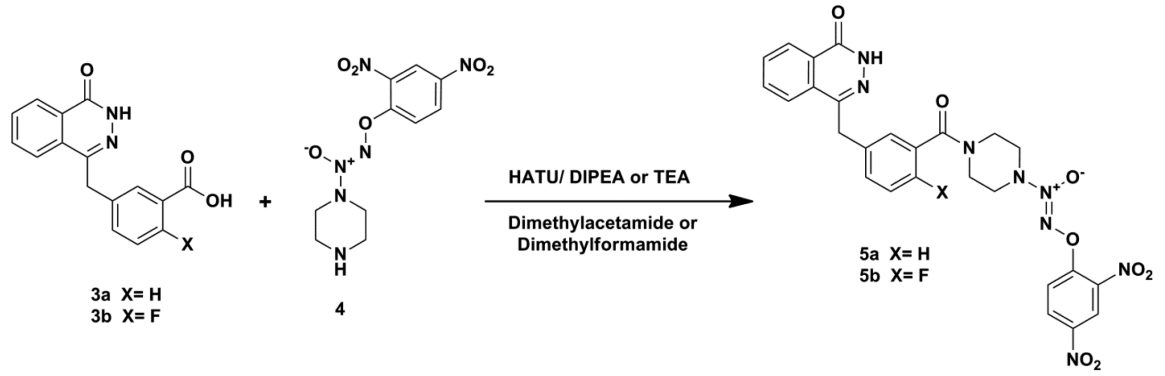

Scheme 3. Activation of 5b in the Presence of 4 mM GSH

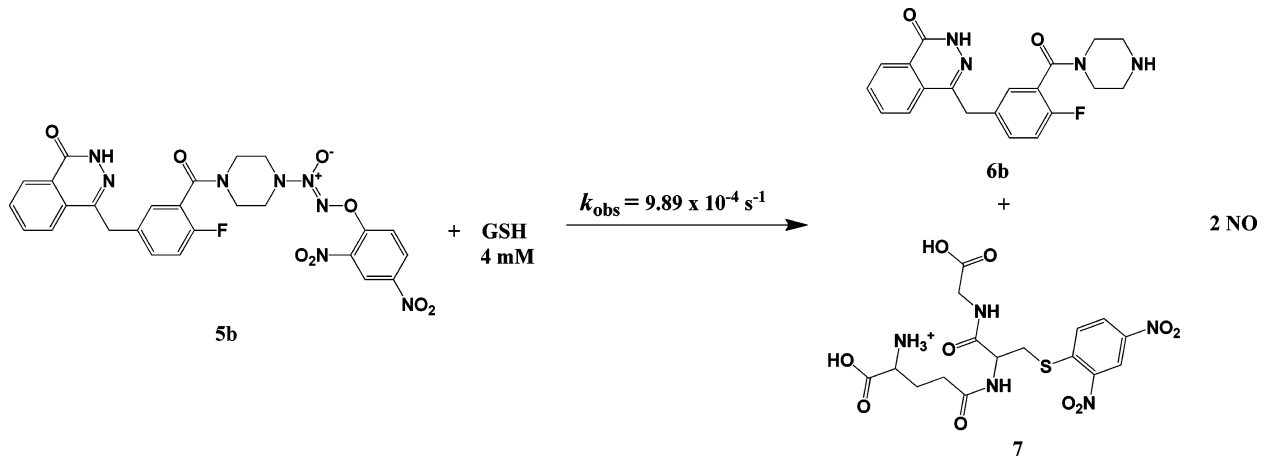

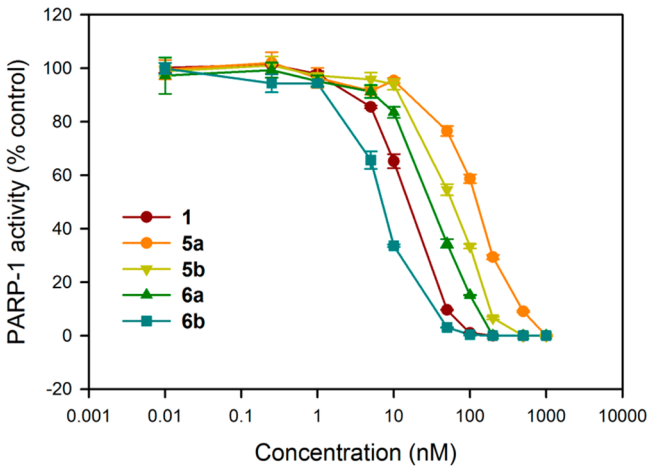

Figure 1. Inhibition of PARP-1 enzyme activity by **5a**, **5b**, **6a**, and **6b**, compared with **1**. Inhibitor concentrations were tested in the range 0.01 nM to 1 μM.

Table 1. Antiproliferative Activities of NO-Releasing PARP-1 Inhibitor Prodrugs Compared with 1 in NSCLC Cells

	IC$_{50}$ ± SD (μM)		
cell line	5a	5b	1
H1568	6.5 ± 0.2	3.0 ± 0.1	36 ± 7.7
H1703	6.8 ± 0.3	4.3 ± 0.3	20 ± 4.2
H441	8.1 ± 0.8	4.5 ± 0.3	28 ± 2.5
H1693	5.3 ± 0.4	5.4 ± 1.2	19 ± 1.4
H2122	11.2 ± 1.8	7.5 ± 0.4	38 ± 4.4
H322M	9.0 ± 1.1	7.9 ± 0.8	50 ± 7.6
H1355	11.4 ± 1.3	8.2 ± 1.4	33 ± 2.6
H23	7.5 ± 0.6	8.4 ± 0.4	10 ± 1.2
H2030	13.8 ± 2.7	9.2 ± 1.1	34 ± 0.9
H1944	14.0 ± 1.6	10.5 ± 3.1	25 ± 4.0
H1792	14.0 ± 0.8	12.7 ± 1.5	16 ± 3.7
A549	16.8 ± 2.2	13.5 ± 1.0	28 ± 3.4
H2023	19.4 ± 2.5	15.0 ± 1.3	20 ± 1.0
H460	13.8 ± 1.6	16.4 ± 0.9	12 ± 2.6

evaluated cellular uptake and metabolism of **5b** in A549 NSCLC cells. Cells were treated with **5b** for varying time periods, and cell lysates were analyzed for the presence of the parent compound and its metabolites by LC/MS. The parent compound was not detected at any measured time point including a brief treatment of 5 min (asterisk (∗) in Figure 3). At all time points measured up to 1 h, compound **6b** and arylated GSH metabolite **7** were detected in equally abundant amounts, suggesting very rapid, presumably catalyzed, cellular metabolism (Figure 3).

Lung cancer cells frequently express high levels of GSTP1, the GST isoform that is often overexpressed in cancer cells. We have screened a panel of 20 NSCLC cell lines for the level of expression of GSTP1 protein using Western blot. This experiment confirmed that the enzyme is highly expressed in a majority of NSCLC cell lines, with little to none of the liver-specific A1 isoform (GSTA1) detected (Figure S4). Therefore,

dx.doi.org/10.1021/jm401550d | J. Med. Chem. 2014, 57, 2292−2302

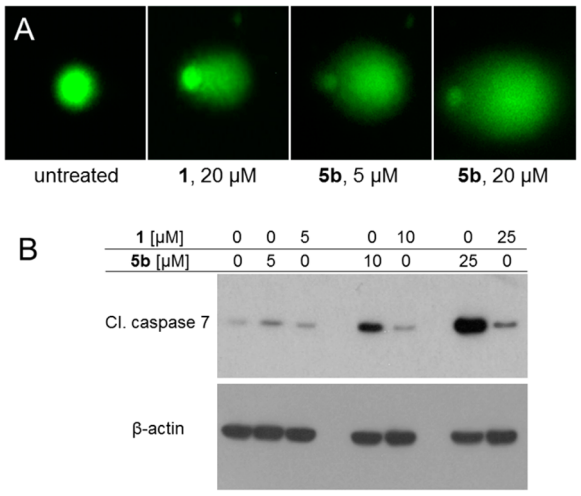

Figure 2. Treatment with NO-releasing PARP-1 inhibitor prodrug **5b** resulted in DNA damage (A), as shown by the Comet assay in H1703 NSCLC cells. The DNA strand break damage caused by **5b** was more extensive than that resulting from **1** treatment. (B) Activation of apoptosis as evidenced by cleavage of caspase 7. Actin served as a loading control.

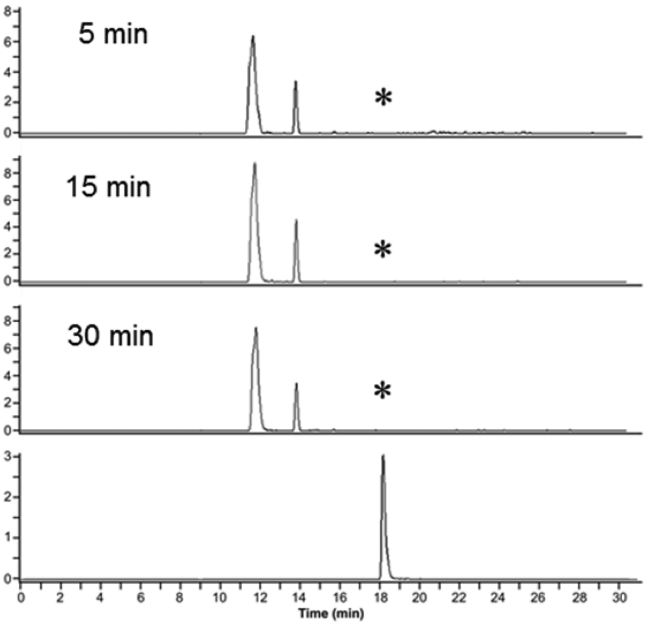

Figure 3. In vitro metabolism of compound **5b**. The human A549 NCSLC cell line was treated with 10 μM **5b**. Then the products were extracted at various time points and analyzed by LC/MS/MS. Shown are extracted ion chromatograms (EICs), which were extracted at various m/z ratios including the $[M + H]^+$ of **6b** (retention time (t_R) of 11.9 min), arylated GSH (**7**, t_R = 13.8 min), and compound **5b** (t_R = 18.2 min) (Scheme 3). The asterisk (∗) indicates where compound **5b** should be, based on the elution profile of a lysate spiked with authentic compound **5b** (bottom panel).

we studied the rate of reaction of **5b** with GSH in the presence of recombinant GSTP1 and found that the reaction was enhanced over 10-fold when the enzyme was present (Table 2, row 3). This strongly suggests that the prodrug, despite its reactivity with GSH alone, will be preferentially activated when GSTP1 is present. Importantly, the presence of GSTP1 did not alter product distribution (Figure S5). Next, **5b** was independently reacted with glutathione in the presence of

Table 2. Selectivity of Prodrugs for GST-Catalyzed Metabolism

compd	$t_{1/2}$ (min) in 4 mM GSH	k_{GSH}/k_{GSH} (mean ± SD)	k_{GSTP}/k_{GSH} (mean ± SD)	k_{GSTA}/k_{GSH} (mean ± SD)
2	2.8 ± 0.02	1 ± 0.001	1.1 ± 0.01	10.5 ± 0.8[a]
8	2.0 ± 0.05	1 ± 0.003	5.4 ± 0.7	3.7 ± 0.08
5b	11.6 ± 0.08	1 ± 0.007	10.6 ± 0.5	20.4 ± 0.7
13	16.0 ± 0.06	1 ± 0.004	13.3 ± 0.4	9.2 ± 0.1

[a]Only two measurements made in the first half-life for the GSTA1 trials.

GSTA1; the A1 isoform was found to be a better catalyst for glutathione attack than GSTP1 (Table 2, row 3). Further synthetic approaches were taken to diminish GSTA1 catalysis.

Synthesis and Metabolism of a Bis-diazeniumdiolated PARP-1 Inhibitor. In an effort to modify the structure of **5b** to make it less susceptible to GSTA1-induced metabolism and to improve its suitability as a substrate for GSTP1, we employed a strategy developed previously to do so with compound **2**.[11] In that case, molecular modeling suggested that adding and reducing steric bulk at different specific locations in the structure of **2** would accomplish this goal. As predicted, compound **8** (PABA/NO, structure in Scheme 4A) was prepared and shown to be metabolized at similar rates by GSTP1 and GSTA1, in contrast to **2**, which was an order of magnitude more efficiently metabolized by GSTA1 (Table 2, rows 1 and 2).

We chose a similar strategy in designing the bis-diazeniumdiolated PARP-1 inhibitor hybrid **13** shown in Scheme 4B as a synthetic target. Thus, Boc-protected piperazine diazeniumdiolate **9** was reacted with aryl fluoride substituted diazeniumdiolate **10** to give adduct **11**, which upon removal of the protecting group gave **12**. This compound contains nucleophilic nitrogen in the piperazine ring that was reacted with **3b** to produce the bis-diazeniumdiolated PARP-1 inhibitor **13**.

Compound **13** was subjected to a similar reactivity and metabolism analysis as **5b**. Not only was compound **13** more stable than **5b** in reactions with GSH alone, but the rates of catalysis suggest that compound **13** is better accommodated in the active site of GSTP1 than that of GSTA1 (Table 2, row 4). Molecular modeling experiments suggested that compound **13** fits nicely into the GSTP1 active site while a steric clash may occur in the GSTA1 active site (Figure 4).

Compound **13** PARP-1 enzyme inhibitory activity in the presence or absence of GSH and GSTP1 was also analyzed.

Mass spectrometric analysis of the cellular metabolism of compound **13** in A549 lung adenocarcinoma cells and U937 human leukemia cells revealed that the compound is metabolized as designed to release NO upon GSH/GST attack. The dearylation of the first diazeniumdiolate moiety results in spontaneous release of NO and frees the PARP-1-inhibitory component. The resulting glutathione conjugate reacts further with GSH, leading to attachment of two glutathionyl substituents to the dinitrophenyl ring (Scheme 4C). Alternatively, the single glutathione conjugates could react with protein thiols instead of GSH, resulting in a protein adduct, in which GSH and the protein's thiol group are covalently cross-linked through the dinitrophenyl ring. This thiol modification (cross-linking glutathionylation) appears to be irreversible and likely plays an important role in mediating the cytotoxic activity of bis-diazeniumdiolates.[12] It is also

dx.doi.org/10.1021/jm401550d | J. Med. Chem. 2014, 57, 2292−2302

Scheme 4. (A) Design Considerations Leading to the Structure-Based Design of 8 as an Improvement over 2 in Terms of Their Suitability as Substrates for GSTP1, (B) Synthesis of NO-Releasing PARP-1 Inhibitor 13, and (C) Metabolism of 13

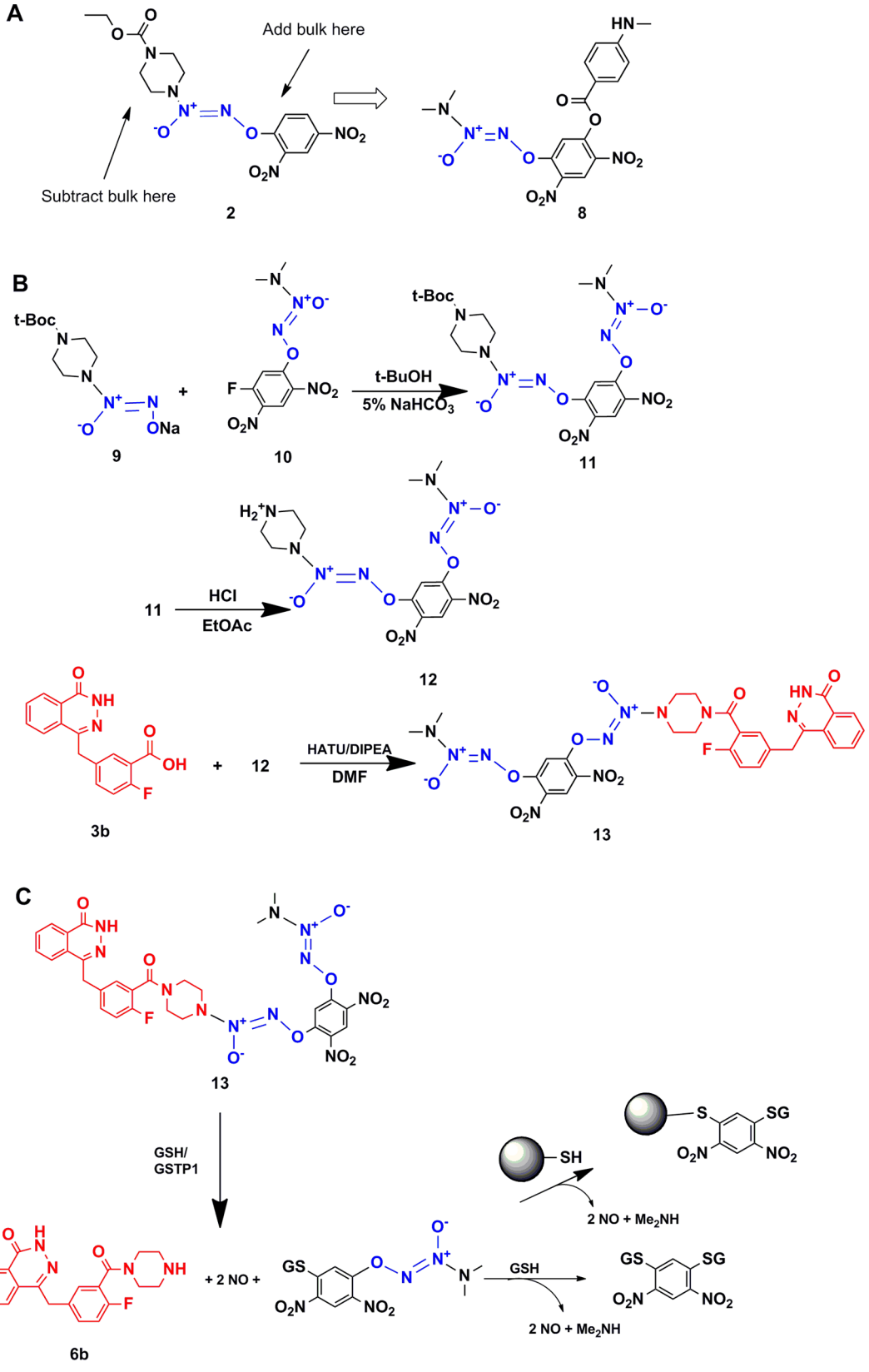

predictable that this irreversible modification will affect proper protein folding, which, if unresolved, leads to the unfolded protein response (UPR) and endoplasmic reticulum (ER) stress.

dx.doi.org/10.1021/jm401550d | J. Med. Chem. 2014, 57, 2292−2302

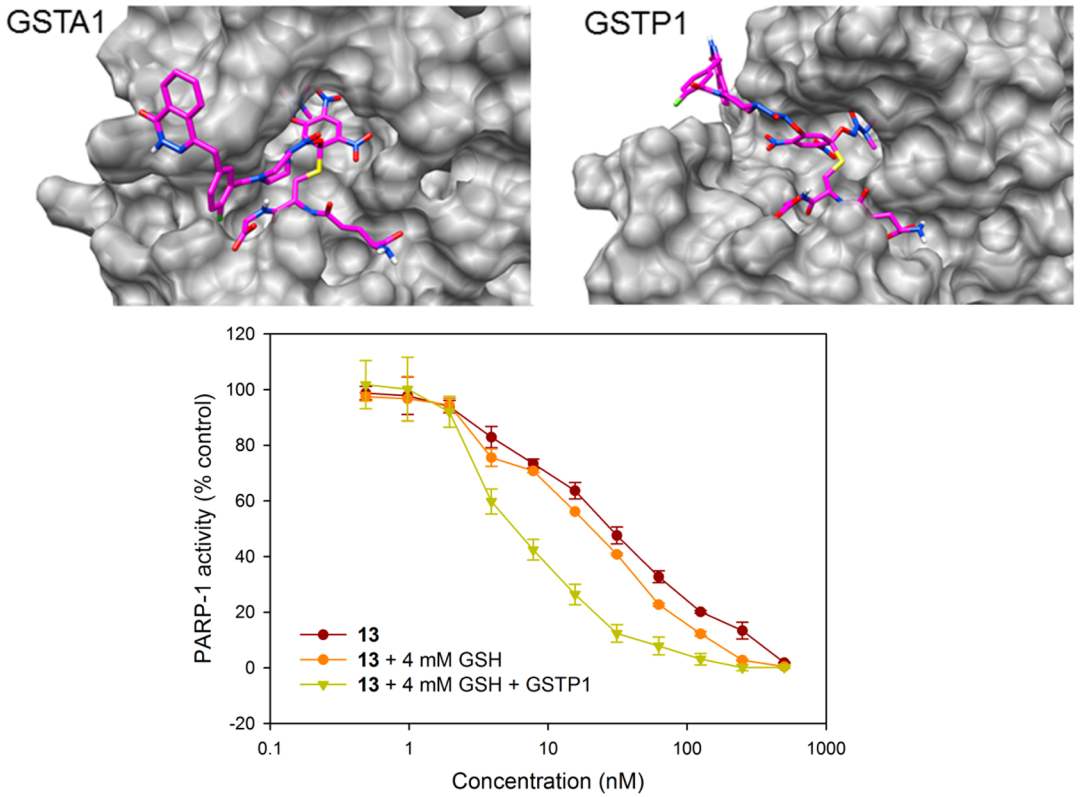

Figure 4. Top panels: Transition state modeling of the **13**−glutathione adduct in the GSTA1 and GSTP1 active sites. Bottom panel: Inhibition of PARP-1 enzyme by compound **13** in the presence or absence of GSH/GSTP1. Activated compound is a much better PARP-1 inhibitor than the prodrug.

Induction of Endoplasmic Reticulum Stress by Compound 13. We exploited this hypothesis and found that indeed treatment with **13** results in cellular protein glutathionylation and ER stress (Figure 5A). Treated cells were lysed and processed for immunoblotting under non-reducing conditions, and protein/GSH cross-links were detected with specific antibodies recognizing glutathione conjugated to proteins. As shown in Figure 5A, glutathione attached to protein was detected within 1 h of treatment, and the signal became gradually stronger with time. The decrease in protein/GSH conjugate signal observed at 8 h was only seen upon the onset of apoptosis, as indicated by cleaved PARP (Figure 5A). This essentially irreversible modification consumes GSH and results in a shift in the cellular redox balance toward a more oxidizing environment, generating oxidative/nitrosative stress. ER stress induction was evidenced by phosphorylation of eIF2α and up-regulation of CHOP, BiP, and ATF4 proteins (Figure 5B). Activation of stress kinase p38 was seen within 15 min after treatment with **13** was initiated (Figure 5C) and could be a result of ROS/RNS stress. We have observed rapid and persistent phosphorylation of p38 in U937 leukemia cells upon treatment with compound **2**.[13]

To determine whether the induction of ROS/RNS and stress signaling were associated with cell death, cells were treated with compound **13** and then analyzed by Western blot for markers of apoptosis. Apoptosis was activated through the extrinsic pathway, as evidenced by caspase 8 activation within 6 h of treatment with 1 μM **13** (Figure 5E). Cleaved effector caspases 3 and 7 and cleaved PARP signals were also observed (Figure 5E).

NO-Releasing PARP-1 Inhibitors Compare Favorably with 1 in Vivo. Human lung adenocarcinoma cell line A549, which expresses moderate levels of GSTP1, was chosen for assessment of activity of the prodrugs in vivo against xenografted cells in athymic mice. Compounds **5b** and **13** were chosen for in vivo studies. Both compounds were administered at 92 μmol/kg intravenously two times a week for a 4-week period to assess anticancer activity. Figure 6 shows significant reduction of the tumor growth in animals treated with compound **13** ($P < 0.02$), compared to **1** or saline controls. Compound **5b** reduced growth of tumors to a lesser extent. Importantly, treatment with either controls or diazeniumdiolate-based drugs did not affect body weights (see caption to Figure 6). Tumors from animals in each group were resected and extracted for analysis of metabolites. Both the parent drugs and the liberated PARP-1 inhibitor were detected in some tumors from animals treated with compounds **5b** and **13**, indicating unambiguous delivery of compound to tumors remote from the site of injection.

Combination with Bortezomib. The ubiquitin−proteasome system is critical for the proliferation and survival of cancer cells. Proteasome inhibition has become a very attractive anticancer therapy. Bortezomib (PS-341, **14**) is a boronic acid dipeptide derivative that selectively and potently inhibits the 26S proteasome.[14] It has clinically validated activity against multiple myeloma and has undergone extensive evaluation in NSCLC. Preliminary in vitro studies established that **14** alone induces growth inhibition in several NSCLC cell lines.[15−18] It has been shown that, combined with cytotoxic agents in vitro, **14** enhanced the antitumor effect in NSCLC and other solid

dx.doi.org/10.1021/jm401550d | J. Med. Chem. 2014, 57, 2292−2302

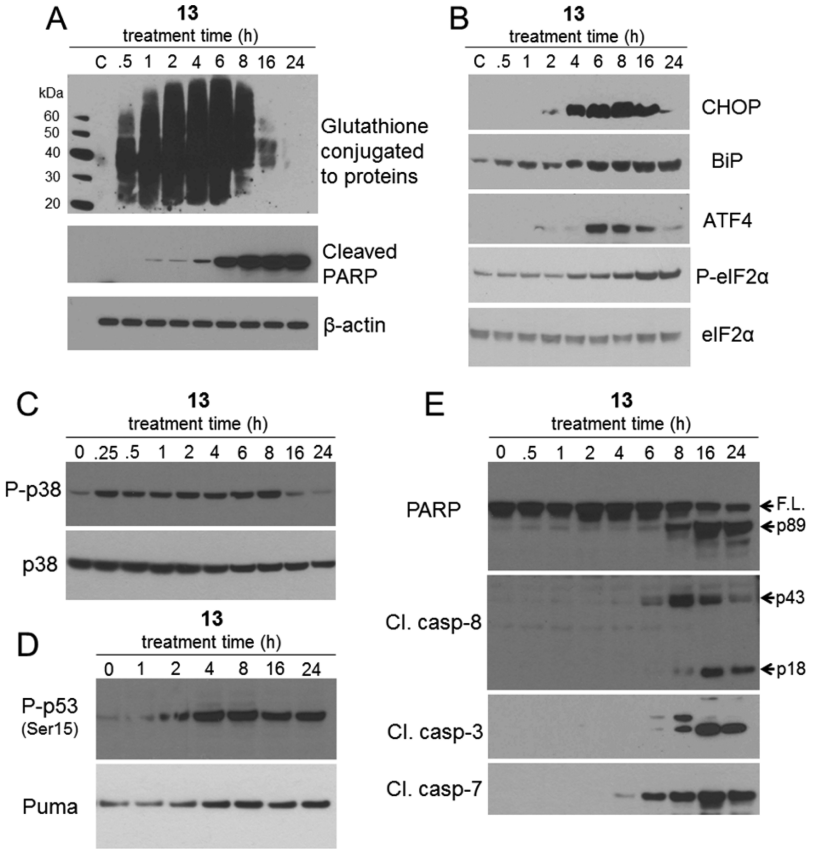

Figure 5. (A) Compound **13** causes cross-linking of GSH to protein thiols (protein glutathionylation) that is irreversible and induces endoplasmic reticulum (ER) stress in A549 lung adenocarcinoma cells (B). (C) Activation of the p38 stress signaling pathway in A549 cells after treatment with **13** occurred rapidly, within 15 min after treatment was initiated, and phosphorylation persisted for 8 h. (D) Tumor suppressor p53 and its effector, Puma, are involved in cells bearing wild-type p53 (A549 NSCLC cell line). Phosphorylation of p53 at Ser15 is an indicator of DNA damage. (E) Treatment with **13** induced the extrinsic apoptosis pathway in A549 cells. Cleavage of caspase 8 and the effector caspases 3 and 7, as well as PARP, was observed: F.L., full length PARP; Cl, cleaved. Images are representative of at least three independent experiments.

tumors,[19] and recently proteasome inhibition as a treatment for NSCLC advanced to clinical trials.[20]

It has previously been shown that the proteasome inhibitor **14** has synergistic activity with compound **2**.[6] **14** induced ROS generation in H460 NSCLC cells.[21] Having shown that cytotoxicity of diazeniumdiolate-based NO-releasing prodrugs correlated with intracellular ROS levels, we hypothesized that co-treatment of lung adenocarcinoma cells with **14** and our prodrugs would result in enhanced cytotoxicity through ROS/RNS stress. Also, proteasome inhibitors are known to induce the unfolded protein response and ER stress. Therefore, a combination of **14** with compound **13**, which causes irreversible, aryl-cross-linking glutathionylation of cellular proteins and induces ER stress, might result in enhanced cytotoxicity. Indeed, combination treatment of **14** and **13** exhibited enhanced toxicity as evaluated by colony forming assay (Figure 7). This promising result suggests that further in vitro and in vivo trials of compound **13** combined with **14** are indicated.

CONCLUSIONS

We have designed prodrugs combining an arylated diazeniumdiolate with a PARP-1 inhibitor to achieve simultaneous delivery of a DNA damaging agent and a DNA repair inhibitor to the cell. Previous work has shown that arylated diazeniumdiolates cause significant DNA strand break damage. Concurrent treatment with a DNA strand break repair inhibitor dramatically exacerbates DNA damage and cytotoxicity. Second-generation molecules have been designed to be preferentially metabolized by cells containing high levels of GSTP1, e.g., cancer cells. We conclude that compound **13**, a bis-diazeniumdiolate, is capable of irreversibly cross-linking GSH to protein thiols, causing the accumulation of misfolded proteins, leading to ER stress (Figure 8). This additional cytotoxic stress adds to the multifaceted proapoptotic mechanisms of arylated diazeniumdiolate action.

EXPERIMENTAL SECTION

General. Starting materials were purchased from Aldrich Chemical Co. (Milwaukee, WI) unless otherwise indicated. NMR spectra were recorded on a Varian UNITY INOVA spectrometer. Chemical shifts (δ) are reported in parts per million (ppm) downfield from tetramethylsilane. Ultraviolet (UV) spectra were recorded on an Agilent model 8453 or a Hewlett-Packard model 8451A diode array spectrophotometer. Elemental analyses were performed by Midwest Microlab (Indianapolis, IN). Chromatography was performed on a Biotage SP1 flash purification system. Prepacked silica gel flash chromatography columns were purchased from Silicycle (Quebec City, Canada) or from Yanazen Science Inc. (San Bruno, CA). Compounds **1**,[10] **2**,[22] **6a**,[10] **6b**,[10] and **8**[11] were prepared as previously described. In addition to NMR, UV, and HPLC with HRMS, CHN combustion analysis was performed to determine purity of compounds. All compounds were ≥95% pure.

Synthesis of 5a. 3-[(4-Oxo-3*H*-phthalazin-1-yl)methyl]benzoic acid, **3a**, was prepared as described by Menear et al.[10] To a slurry of

dx.doi.org/10.1021/jm401550d | J. Med. Chem. 2014, 57, 2292−2302

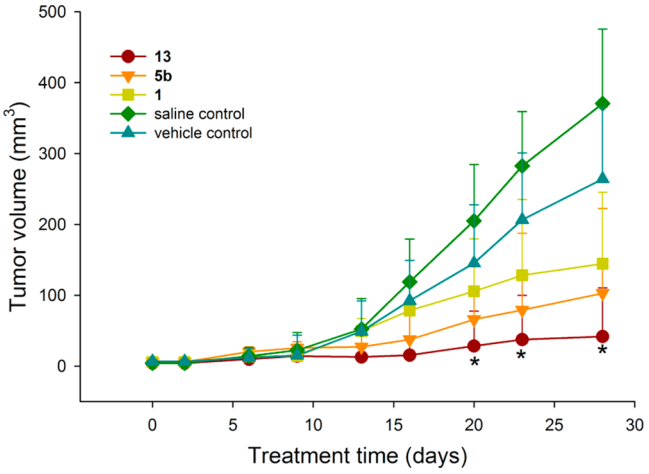

Figure 6. (A) Compound **13** significantly reduced growth of NSCLC cells in vivo. Compounds were administered intravenously at 92 μmol/kg, 2 times a week for 4 weeks, and tumors were measured with a caliper. Values are medians, and the relevant 95% confidence interval bars are shown (Mann−Whitney test). Stars indicate the significance of the differences between **13**-treated and **1**-treated and control mice at each time point. The treatment did not affect body weights. The average body weight for all mice was 22.9 ± 0.31 g (mean ± SE) at the beginning of the experiment. At the termination, the average weights of the control groups were 25.6 ± 0.76 g (n = 12), 25.0 ± 0.78 g (n = 10), and 25.0 ± 0.77 g (n = 11) for **1**, vehicle, and saline control, respectively. The weights of animals treated with **13** were 25.3 ± 0.49 g (n = 10), and those treated with **5b** were 27.7 ± 0.82 g (n = 11).

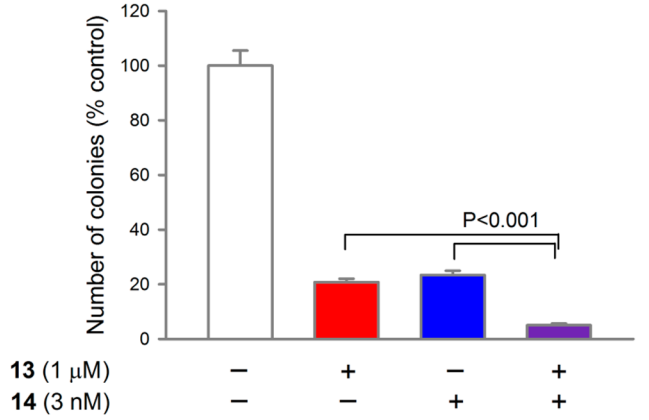

Figure 7. Colony forming assay (A549 cells) indicated enhanced cytotoxicity of the combination of compound **13** with proteasome inhibitor **14**.

557 mg (1.6 mmol) of the hydrochloride salt of **4**,[5] 448 mg (1.6 mmol) of **3a**, and 608 mg (1.6 mmol) of HATU in 5 mL of dimethylacetamide was added 1.02 mL (6 mmol) of diisopropylethylamine. The resulting solution was stirred at room temperature for 1 h, followed by addition of 40 mL of water. The resulting precipitate was collected by filtration and recrystallized from ethanol, giving 827 mg of an off-white solid: mp 114−117 °C; UV (acetonitrile) λ_{max} 294 nm (ε = 18.9 mM^{-1} cm^{-1}); ^{1}H NMR (DMSO-d_6) δ 3.63−3.68 (m, 8H), 4.38 (s, 2H), 7.28−7.30 (m, 1H), 7.39−7.46 (m, 3H), 7.81−7.98 (m, 4H), 8.26 (d, 1H) J = 7.4 Hz, 8.56−8.59 (dd, 1H) J = 2.7, 7.4 Hz, 8.88 (d, 1H) J = 2.7 Hz, 12.06 (s, 1H); ^{11}C NMR (DMSO-d_6) δ 37.7, 50.2, 116.5, 122.5, 125/6, 125.9, 126.5, 127.8, 128.3, 129.2, 129.6, 130.2, 130.7, 132.0, 133.9, 135.6, 137.3, 138.93, 142.6, 145.3, 153.2, 159.8, 169.4; HRMS (ESI) m/z calculated for $C_{26}H_{23}N_8O_8$ [M + H]$^+$ = 575.1639, found 575.1548, Δ ppm = 1.5. Anal. Calcd for $C_{26}H_{22}N_8O_8 \cdot H_2O$: C, 52.70; H, 4.08; N, 18.91. Found: C, 52.66; H, 3.73, N, 18.50.

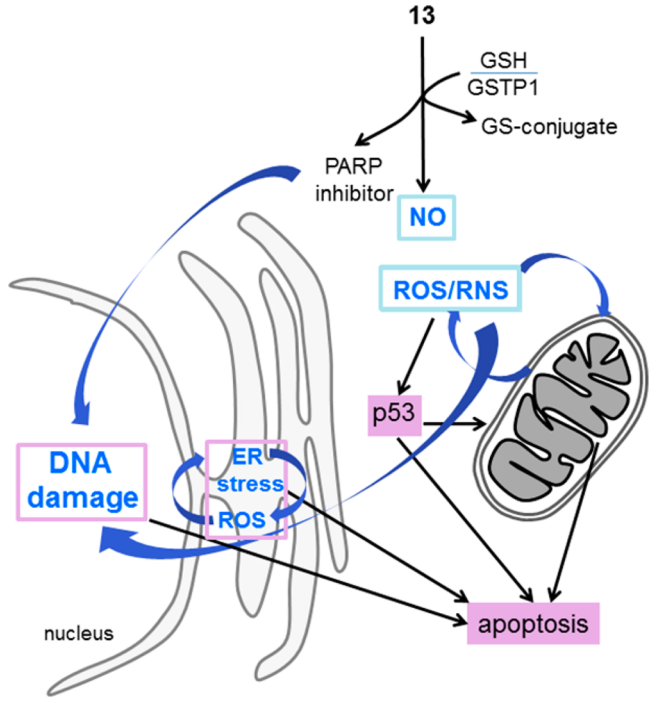

Figure 8. Mechanism of action of bis-diazeniumdiolate/PARP-1 inhibitor, compound **13**.

Synthesis of 5b. A solution of 685 mg (2.3 mmol) of **3b**[10] in 30 mL of *N*,*N*-dimethylformamide was cooled to 4 °C. HATU (950 mg, 2.5 mmol) was added, and the resulting slurry was stirred under nitrogen. A solution of 765 mg (2.19 mmol) of **4**[5] and 753 μL (5 mmol) of diisopropylethylamine in 60 mL of dimethylformamide was added, and the resulting solution was stirred at room temperature overnight. The solution was cooled to 4 °C and ice−water (200 mL) was added, giving a solid precipitate. The product was collected by filtration, washed with water, and allowed to dry to give 1.3 g of crude material. Recrystallization from ethanol afforded 853 mg of pure **5b**: mp 150−153 °C; UV (acetonitrile) λ_{max} 295 nm (ε = 20.5 mM^{-1} cm^{-1}); ^{1}H NMR (DMSO-d_6) δ 3.41 (b, 1H), 3.58 (b, 1H), 3.72 (b, 1H), 3.84 (b, 1H), 4.33 (s, 2H), 7.25 (t, 1H) J = 9.0 Hz, 7.37−7.46 (m, 2H), 7.82 (t, 2H) J = 9.0 Hz, 7.87−7.97 (m, 3H), 8.24 (d, 1H) J = 7.8 Hz, 8.54−8.57 (dd, 1H) J = 2.4, 7.8 Hz, 8.86 (d, 1H) J = 2.4 Hz, 12.58 (s, 1H); ^{13}C NMR (DMSO-d_6) δ 36.9, 45.2, 50.5, 116.9, 118.52, 119.5, 122.6, 124.0, 125.8, 126.5, 127.9, 129.3, 130.2, 131.9, 132.6, 133.9, 135.2, 137.3, 142.6, 145.2, 154.1 (d) J_{C-F} = 246 Hz, 159.8, 164.4; HRMS (ESI) m/z calculated for $C_{26}H_{22}FN_8O_8$ [M + H]$^+$ = 593.1545, found 593.1538, Δ ppm = 1.1. Anal. Calcd for $C_{26}H_{21}FN_8O_8 \cdot H_2O$: C, 51.15; H, 3.80; N, 18.35; F, 3.11. Found: C, 51.45; H, 3.70, N, 18.41; F, 3.42.

Synthesis of Compound 11. A partial solution of 2.52 g (0.0087 mol) of O^2-(2,4-dinitro-5-fluorophenyl) 1-(*N*,*N*-dimethylamino)-diazen-1-ium-1,2-diolate (**10**)[5] in 120 mL of *tert*-butanol was stirred at room temperature. A solution of 2.34 g (0.0087 mol) of sodium 1-[4-(*tert*-butoxycarbonyl)piperazin-1-yl]diazen-1-ium-1,2-diolate (**9**)[23] in 120 mL of 5% aqueous sodium bicarbonate was added gradually through a pressure equalizing addition funnel, and the resulting mixture was stirred at room temperature overnight. The reaction mixture was treated with 150 mL of water and the resulting yellow solid was collected by filtration, washed with water, and dried to give 1.33 g of product. The material was placed on a silica gel column and eluted with hexane/ethyl acetate to give 3.6 g (80%) of **11** as a yellow powder: mp 123−125 °C; UV (acetonitrile) λ_{max} 292 nm (ε = 23 mM^{-1} cm^{-1}); ^{1}H NMR ($CDCl_3$) δ 1.49 (s, 9H), 3.28 (s, 6H), 3.60−3.61 (m, 4H), 3.65−3.67 (m, 4H), 7.57 (s, 1H), 8.86 (s, 1H); ^{13}C NMR ($CDCl_3$) δ 28.3, 41.8, 50.5, 81.0, 105.3, 125.5, 154.2, 154.3.

dx.doi.org/10.1021/jm401550d | J. Med. Chem. 2014, 57, 2292−2302

Anal. Calcd for $C_{17}H_{25}N_9O_{10}$: C, 39.61; H, 4.89; N, 24.46. Found: C, 39.44; H, 4.79; N, 24.09.

Synthesis of Compound 12 as the Hydrochloride Salt. To a solution of 3.6 g (0.007 mol) of **11** in 300 mL of ethyl acetate was added 70 mL of 2 M HCl in ether. The resulting solution was stirred at room temperature. The hydrochloride salt precipitated from the solution gradually over a 72 h period. The product was collected by filtration, washed with ethyl acetate, and allowed to dry, giving 3.1 g (98%) of **12**: mp 135−137 °C; UV (ethanol) λ_{max} 288 nm (ε = 28 mM^{-1} cm^{-1}); ^1H NMR (DMSO-d_6) δ 3.26 (s, 6H), 3.33−3.35 (b, 9H; 4H for piperazine, 5H for water), 3.89−3.91 (m, 4H), 7.82 (s, 1H), 8.90 (s, 1H), 8.41 (b, 2H); ^{13}C NMR (DMSO-d_6) δ 41.6, 47.2, 105.6, 125.7, 131.5, 131.9, 153.6, 154.1. This salt was used for the next step without further purification.

Synthesis of Compound 13. To a solution of 2.05 g (0.006 87 mol) of **3b**[10] and 2.85 g (0.0075 mol) of HATU in 150 mL of *N*,*N*-dimethylformamide was added 2.6 mL (0.015 mol) of DIPEA. To the solution was gradually added 3.1 g (0.006 87 mol) of **12** in 150 mL of *N*,*N*-dimethylformamide, and the resulting solution was stirred at room temperature overnight. The solution was treated with 250 mL of cold aqueous ammonium chloride solution, and the resulting precipitate was collected by filtration and washed with water. The solid containing water and dimethylformamide was taken up in dichloromethane, dried over sodium sulfate, filtered through a layer of anhydrous magnesium sulfate, and evaporated in vacuo. The yellow moist solid was triturated with ether to give, after filtration, 2.16 g of **13**. Recrystallization from ethanol gave a product of 88% purity. Purification was carried out with preparative HPLC: mp 122−125 °C; UV (0.2% DMSO/ethanol) λ_{max} 287 nm (ε = 32 mM^{-1} cm^{-1}); ^1H NMR (acetone-d_6) δ 3.30 (s, 6H), 3.58−3.97 (m, 8H), 7.14−7.22 (m, 1H), 7.44−7.54 (m, 2H), 7.79 (s, 1H), 7.80−7.88 (m, 1H), 7.94−7.96 (m, 2H), 8.32−8.34 (m, 1H), 8.86 (s, 1H), 11.75 (s, 1H); ^{13}C NMR (acetone-d_6) δ 37.9, 41.7, 51.0, 51.2, 105.5, 110.75, 116.5, 116.9, 124.8, 125.9, 126.4, 127.2, 129.5, 132.1, 134.1, 136.0, 145.6, 153.4, 155.1, 155.6 (d) J_{C-F} = 201.0 Hz, 160.3, 165.1. For further decomposition and biological screening, a portion of the compound was purified on a Phenomenex Luna C18 column, 3 μm, 150 mm × 2.0 mm, with a gradient consisting of water and acetonitrile containing 0.1% formic acid. HRMS (ESI) *m*/*z* calculated for $C_{28}H_{27}FN_{11}O_{10}$ $[M + H]^+$ = 696.1921, found 696.1928, Δ ppm = 0.96. Anal. Calcd for $C_{28}H_{26}N_{11}FO_{10}\cdot H_2O$: C, 47.13; H, 3.95; F, 2.66; N, 21.59. Found: C, 47.14; H, 4.08; F, 2.73; N, 21.45.

Determination of Intracellular Reactive Oxygen/Nitrogen Species and Nitric Oxide. Intracellular levels of reactive oxygen/nitrogen species were quantified by oxidation of the ROS/RNS-sensitive fluorophore 5-(and -6)-chloromethyl-2′,7′-dichlorodihydrofluorescein diacetate (DCF-DA, Invitrogen, Carlsbad, CA). Cells growing on six-well plates (6 × 10^5/well) were loaded with 5 μM DCF-DA in Hanks' balanced salt solution (HBSS) at 37 °C and 5% CO_2. After 30 min of incubation, HBSS containing the probe was removed, cells were rinsed with HBSS, and 3 mL of fresh HBSS was added to each well followed by addition of compounds (10 μM) or DMSO as a control. After 60 min the cells were collected by scraping in HBSS, and DCF fluorescence was measured by using a PerkinElmer Life and Analytical Sciences (Waltham, MA) LS50B luminescence spectrometer with the excitation source at 488 nm and emission at 530 nm.

The intracellular level of nitric oxide and its oxidation products after treatment with compounds was estimated by using the fluorophore 4-amino-5-methylamino-2,7-difluorofluorescein (DAF-FM) diacetate (Invitrogen). Cells growing in six-well plates were loaded with 2.5 μM DAF-FM diacetate in HBSS at 37 °C and 5% CO_2. After 30 min of incubation the cells were rinsed with HBSS to remove excess probe. Test compounds in fresh HBSS were added to the cells at 10 μM final concentration. After 30 min of incubation, the fluorescence of the benzotriazole derivative formed on DAF-FM's reaction with aerobic NO was analyzed by using a PerkinElmer Life and Analytical Sciences LS50B luminescence spectrometer with the excitation source at 495 nm and emission at 515 nm. All experiments were performed at least three times, each time at least in triplicate.

PARP Inhibition Assay. PARP enzyme inhibition was measured using an HT Universal Colorimetric 96-well PARP assay kit (Trevigen, Gaithersburg, MD), according to the manufacturer's protocol with the following small modifications: When inhibitory activities of activated prodrugs were studied, GSH (4 mM) was added in the presence and absence of GSTP1 in PBS, pH 7.4. Reactions were initiated by the addition of prodrug after a 10 min incubation at 37 °C and carried out for another 10 min. Substrate concentrations were 10 μM with a GSTP1 concentration of 40 nM. The absorbance at 450 nm was measured.

Cell Culture and Proliferation Assay. Cell lines were obtained from the American Type Culture Collection (Manassas, VA) and cultured according to the supplier's protocol. For proliferation assays, cells were seeded at 1 × 10^4 per well (H1693, H322M, H1703, H1944, H1355, H2122, H441, H1568) or 5 × 10^3 per well (H460, H1792, A549, H2023, H2030, H23) in 96-well plates and allowed to adhere for 24 h. Compounds were prepared as 10 mM stock solutions in DMSO. Increasing drug concentrations in 10 μL of PBS were added to 100 μL of the culture medium and incubated for 72 h. The MTT assay (Promega, Madison, WI) was performed according to the manufacturer's protocol. Each concentration was represented in six repeats, and the screening was performed as at least two independent experiments. IC_{50} values were calculated by using Sigma Plot software (Systat Software, Inc., San Jose, CA).

Catalysis of NO-Releasing PARP Inhibitor Activation by Glutathione S-Transferase. Kinetic experiments were performed at 37 °C using a standard UV−visible spectrophotometer. GSH (4 mM) was added in the presence and absence of GSTP1 or GSTA1 in 0.1 M phosphate buffer solution, pH 7.4, containing 50 μM diethylenetriaminepentaacetic acid (DTPA). Reactions were initiated by the addition of substrate after the GSH-containing buffer and enzyme reached thermal equilibrium. Typical substrate concentrations were 10 μM with a GST concentration of 40 nM. In each experiment the data were analyzed at 302 nm and the rate was derived by fitting the data to an exponential curve typical for first order processes.

In Vitro Metabolism of Compounds 5b and 13. The metabolism of each compound was studied in the human A549 NSCLC cell line and the human U937 leukemia cell line. In each case cells were plated in 75 cm^2 flasks and incubated overnight at 37 °C. The A549 cell line was treated with 10 μM of each compound and incubated for varying time points. At each time point the cells were lysed via scraping in 400 μL of 10 mM HCl and 400 μL of HPLC grade acetonitrile. The U937 cell line was treated with 5 μM of each compound and by two cycles of freeze (−80 °C) and thaw (37 °C) in 400 μL of 10 mM HCl and 400 μL of HPLC grade acetonitrile. To each lysate was added 200 μL of a 5% 5-sulfosalicylic acid solution. The precipitate was removed by centrifugation at 12000*g* for 15 min, followed by syringe filtration of the supernatant and analysis by LC/MS.

The system used for analysis is an Agilent 1200 HPLC instrument coupled with an Agilent 6520 accurate-mass quadrupole time-of-flight (Q-TOF) LC/MS/MS instrument. Positive ions were generated with the Agilent multimode source in mixed mode. Separations were performed on a Phenomenex Luna column, C18 5 μm, 2.1 mm × 150 mm, at a flow rate of 0.2 mL/min under H_2O/acetonitrile/0.1% formic acid gradient conditions.

Comet Assay. The alkaline comet assay was performed as described.[24]

Molecular Modeling. Transition state modeling of the **13**−glutathione adduct in the GSTA1 and GSTP1 active sites was carried out as described.[25] Briefly, the initial models of the Meisenheimer complex of compound **13** (GS**13**$^-$) bound to GSTP1 or GSTA1 was built on the basis of the GSTCD$^-$ in the GSTP1·GSTCD$^-$ structure (PDB entry 1AQX)[26] or in the GSTA1·GSTCD$^-$ model complex.[25] The initial GSTA1·GSTCD$^-$ model complex was built on the basis of the crystal structures of the GSTCD$^-$ found in the active sites of GSTM1 (PDB entry 4GST) and GSTP1 (PDB entry 1AQX), and then it was docked into the active site of GSTA1 in complex with the GSH adduct of ethacrynic acid (PDB entry 1GSE). The GSTP1·GS**13**$^-$ and GSTA1·GS**13**$^-$ complexes built in dimeric forms because

GSH interacts with the side chains from both subunits of GST. The dimeric model complexes were subject to geometry optimization using the MacroModel module of Schrödinger, LLC (MacroModel, version 9.6).[27] OPLS_2005 force field with efficient continuum solvation models was used during energy minimization.

Immunoblot Analysis. Western blot analysis was performed as described.[7] Most of the primary antibodies were from Cell Signaling Technology (Danvers, MA), with the exception of ATF3 which was from Santa Cruz Biotechnology (Santa Cruz, CA).

To analyze for glutathionylation of cellular proteins, lysates were separated by gel electrophoresis (4−12% NuPAGE gel) under nonreducing conditions, transferred to PVDF membranes, and probed with anti-glutathione conjugated to protein monoclonal antibody (Virogen).

Establishment of Xenograft Tumors and Drug Injections. Human lung adenocarcinoma cell line A549 was obtained from the American Type Culture Collection and cultured in RPMI 1640 medium with 10% fetal bovine serum, according to the cell supplier's protocol, for a maximum of four passages before use. Cells were harvested at 70−80% confluence, washed with phosphate buffered saline, suspended in phosphate buffered saline, and implanted subcutaneously at 5×10^6 cells/0.2 mL into NCr nu/nu athymic mice, obtained from Charles River. Frederick National Laboratory for Cancer Research is accredited by AAALAC International and follows the Public Health Service Policy for the Care and Use of Laboratory Animals. Animal care was provided in accordance with the procedures outlined in the "Guide for Care and Use of Laboratory Animals" (National Research Council, 1996; National Academy Press, Washington, DC). When the tumors reached approximately 3 mm × 3 mm, the mice were distributed randomly into groups of 12 for treatment.

Compounds were injected into the tail veins of the mice, at 92 μmol/kg body weight (in 20 μL of DMSO solution), 2 times per week for 4 weeks. Control groups were treated with saline or DMSO. Mice were weighed, and tumors were measured 2 times per week. Tumor volumes in mm^3 were estimated by the formula ($^{\pi}/_{2}$ × length × width^2). Mice were euthanized almost immediately after the last treatment. Blood was collected under isoflurane anesthesia into Eppendorf tubes containing 50% acetonitrile/10 mM HCl for drug metabolite analysis. Tumors were also removed and frozen immediately for drug metabolite analysis.

Statistical Analysis. All experiments (with the exception of the proliferation assay and in vivo study) were performed at least three times, each time at least in triplicate. Results are presented as averages ± SE. Statistical tests were carried out by using Instat, version 3.00 (GraphPad Software Inc., San Diego, CA). Pairwise comparisons included the *t* test, with the Welch correction or application of the Mann−Whitney test as appropriate. Significance of correlations was assessed by the Pearson linear correlation or the Spearman test as appropriate.

■ ASSOCIATED CONTENT

Supporting Information

Activation of **5b** in the presence of 4 mM GSH, correlations of IC_{50} of **5b** with ROS, PRX1, and OGG1, data showing ROS/RNS stress in cells treated with **5a** and **5b**, GSTP1 and GSTA1 protein expression levels in NSCLC cell lines, product distribution in the reaction of **5b** with GSH in the presence or absence of GSTP1, and NMR spectra of new compounds. This material is available free of charge via the Internet at http://pubs.acs.org.

■ AUTHOR INFORMATION

Corresponding Author

*Phone: 301-846-1246. Fax: 301-846-5946. E-mail: maciaga@mail.nih.gov.

Notes

The authors declare no competing financial interest.

■ ACKNOWLEDGMENTS

We thank Dr. Sergey Tarasov and Marzena A. Dyba of the Biophysics Resource in the Structural Biophysics Laboratory, NCI-Frederick, for assistance with the high resolution mass spectrometry studies. This project has been funded in part with federal funds from the National Cancer Institute, National Institutes of Health, under Contract HHSN26120080001E. The content of this publication does not necessarily reflect the views or policies of the Department of Health and Human Services, nor does mention of trade names, commercial products, or organizations imply endorsement by the U.S. Government. This research was supported [in part] by the Intramural Research Program of the NIH, National Cancer Institute, Center for Cancer Research.

■ ABBREVIATIONS USED

NO, nitric oxide; JS-K, O^2-(2,4-dinitrophenyl) 1-[(4-ethoxycarbonyl)piperazin-1-yl]diazen-1-ium-1,2-diolate; NSCLC, non-small-cell lung cancer; GST, glutathione S-transferase; GSH, glutathione; DMSO, dimethyl sulfoxide; HBSS, Hanks's balanced salt solution; TBS-T, Tris-buffered saline−Tween-20; PBS, phosphate buffered saline; MTT, 3-(4,5-dimethylthiazol-2-yl)-2,5-diphenyltetrazolium bromide

■ REFERENCES

(1) Samol, J.; Ranson, M.; Scott, E.; Macpherson, E.; Carmichael, J.; Thomas, A.; Cassidy, J. Safety and tolerability of the poly(ADP-ribose) polymerase (PARP) inhibitor, olaparib (AZD2281) in combination with topotecan for the treatment of patients with advanced solid tumors: a phase I study. *Invest. New Drugs* **2012**, *30*, 1493−1500.

(2) Khan, O. A.; Gore, M.; Lorigan, P.; Stone, J.; Greystoke, A.; Burke, W.; Carmichael, J.; Watson, A. J.; McGown, G.; Thorncroft, M.; Margison, G. P.; Califano, R.; Larkin, J.; Wellman, S.; Middleton, M. R. A phase I study of the safety and tolerability of olaparib (AZD2281, KU0059436) and dacarbazine in patients with advanced solid tumours. *Br. J. Cancer* **2011**, *104*, 750−755.

(3) Rajan, A.; Carter, C. A.; Kelly, R. J.; Gutierrez, M.; Kummar, S.; Szabo, E.; Yancey, M. A.; Ji, J.; Mannargudi, B.; Woo, S.; Spencer, S.; Figg, W. D.; Giaccone, G. A phase I combination study of olaparib with cisplatin and gemcitabine in adults with solid tumors. *Clin. Cancer Res.* **2012**, *18*, 2344−2351.

(4) Shami, P. J.; Saavedra, J. E.; Wang, L. Y.; Bonifant, C. L.; Diwan, B. A.; Singh, S. V.; Gu, Y.; Fox, S. D.; Buzard, G. S.; Citro, M. L.; Waterhouse, D. J.; Davies, K. M.; Ji, X.; Keefer, L. K. JS-K, a glutathione/glutathione S-transferase activated nitric oxide donor of the diazeniumdiolate class with potent antineoplastic activity. *Mol. Cancer Ther.* **2003**, *2*, 409−417.

(5) Shami, P. J.; Saavedra, J. E.; Bonifant, C. L.; Chu, J.; Udupi, V.; Malaviya, S.; Carr, B. I.; Kar, S.; Wang, M.; Jia, L.; Ji, X.; Keefer, L. K. Antitumor activity of JS-K [O^2-(2,4-dinitrophenyl) 1-[(4-ethoxycarbonyl)piperazin-1- yl]diazen-1-ium-1,2-diolate] and related O^2-aryl diazeniumdiolates in vitro and in vivo. *J. Med. Chem.* **2006**, *49*, 4356−4366.

(6) Kiziltepe, T.; Hideshima, T.; Ishitsuka, K.; Ocio, E. M.; Raje, N.; Catley, L.; Li, C. Q.; Trudel, L. J.; Yasui, H.; Vallet, S.; Kutok, J. L.; Chauhan, D.; Mitsiades, C. S.; Saavedra, J. E.; Wogan, G. N.; Keefer, L. K.; Shami, P. J.; Anderson, K. C. JS-K, a GST-activated nitric oxide generator, induces DNA double-strand breaks, activates DNA damage response pathways, and induces apoptosis in vitro and in vivo in human multiple myeloma cells. *Blood* **2007**, *110*, 709−718.

(7) Maciag, A. E.; Chakrapani, H.; Saavedra, J. E.; Morris, N. L.; Holland, R. J.; Kosak, K. M.; Shami, P. J.; Anderson, L. M.; Keefer, L. K. The nitric oxide prodrug JS-K is effective against non-small-cell lung

cancer cells in vitro and in vivo: involvement of reactive oxygen species. *J. Pharmacol. Exp. Ther.* **2011**, *336*, 313−320.
(8) Nandurdikar, R. S.; Maciag, A. E.; Holland, R. J.; Cao, Z.; Shami, P. J.; Anderson, L. M.; Keefer, L. K.; Saavedra, J. E. Structural modifications modulate stability of glutathione-activated arylated diazeniumdiolate prodrugs. *Bioorg. Med. Chem.* **2012**, *20*, 3094−3099.
(9) Weyerbrock, A.; Osterberg, N.; Psarras, N.; Baumer, B.; Kogias, E.; Werres, A.; Bette, S.; Saavedra, J. E.; Keefer, L. K.; Papazoglou, A. JS-K, a glutathione S-transferase-activated nitric oxide donor with antineoplastic activity in malignant gliomas. *Neurosurgery* **2012**, *70*, 497−510.
(10) Menear, K. A.; Adcock, C.; Boulter, R.; Cockcroft, X. L.; Copsey, L.; Cranston, A.; Dillon, K. J.; Drzewiecki, J.; Garman, S.; Gomez, S.; Javaid, H.; Kerrigan, F.; Knights, C.; Lau, A.; Loh, V. M., Jr.; Matthews, I. T.; Moore, S.; O'Connor, M. J.; Smith, G. C.; Martin, N. M. 4-[3-(4-Cyclopropanecarbonylpiperazine-1-carbonyl)-4-fluorobenzyl]-2*H*-phthalazin-1-one: a novel bioavailable inhibitor of poly(ADP-ribose) polymerase-1. *J. Med. Chem.* **2008**, *51*, 6581−6591.
(11) Saavedra, J. E.; Srinivasan, A.; Buzard, G. S.; Davies, K. M.; Waterhouse, D. J.; Inami, K.; Wilde, T. C.; Citro, M. L.; Cuellar, M.; Deschamps, J. R.; Parrish, D.; Shami, P. J.; Findlay, V. J.; Townsend, D. M.; Tew, K. D.; Singh, S.; Jia, L.; Ji, X.; Keefer, L. K. PABA/NO as an anticancer lead: analogue synthesis, structure revision, solution chemistry, reactivity toward glutathione, and in vitro activity. *J. Med. Chem.* **2006**, *49*, 1157−1164.
(12) Holland, R. J.; Maciag, A. E.; Kumar, V.; Shi, L.; Saavedra, J. E.; Prud'homme, R. K.; Chakrapani, H.; Keefer, L. K. Cross-linking protein glutathionylation mediated by O^2-arylated bis-diazeniumdiolate "double JS-K". *Chem. Res. Toxicol.* **2012**, *25*, 2670−2677.
(13) Maciag, A. E.; Holland, R. J.; Cheng, R. Y-S.; Rodriguez, L. G.; Saavedra, J. E.; Anderson, L. M.; Keefer, L. K. Nitric oxide-releasing prodrug triggers cancer cell death through deregulation of cellular redox balance. *Redox Biol.* **2013**, *1*, 115−124.
(14) Adams, J.; Palombella, V. J.; Sausville, E. A.; Johnson, J.; Destree, A.; Lazarus, D. D.; Maas, J.; Pien, C. S.; Prakash, S.; Elliott, P. J. Proteasome inhibitors: a novel class of potent and effective antitumor agents. *Cancer Res.* **1999**, *59*, 2615−2622.
(15) Ling, Y. H.; Liebes, L.; Ng, B.; Buckley, M.; Elliott, P. J.; Adams, J.; Jiang, J. D.; Muggia, F. M.; Perez-Soler, R. PS-341, a novel proteasome inhibitor, induces Bcl-2 phosphorylation and cleavage in association with G2-M phase arrest and apoptosis. *Mol. Cancer Ther.* **2002**, *1*, 841−849.
(16) Ling, Y. H.; Liebes, L.; Jiang, J. D.; Holland, J. F.; Elliott, P. J.; Adams, J.; Muggia, F. M.; Perez-Soler, R. Mechanisms of proteasome inhibitor PS-341-induced G(2)-M-phase arrest and apoptosis in human non-small cell lung cancer cell lines. *Clin. Cancer Res.* **2003**, *9*, 1145−1154.
(17) Mortenson, M. M.; Schlieman, M. G.; Virudachalam, S.; Bold, R. J. Effects of the proteasome inhibitor bortezomib alone and in combination with chemotherapy in the A549 non-small-cell lung cancer cell line. *Cancer Chemother. Pharmacol.* **2004**, *54*, 343−353.
(18) Yang, Y.; Ikezoe, T.; Saito, T.; Kobayashi, M.; Koeffler, H. P.; Taguchi, H. Proteasome inhibitor PS-341 induces growth arrest and apoptosis of non-small cell lung cancer cells via the JNK/c-Jun/AP-1 signaling. *Cancer Sci.* **2004**, *95*, 176−180.
(19) Denlinger, C. E.; Rundall, B. K.; Jones, D. R. Proteasome inhibition sensitizes non-small cell lung cancer to histone deacetylase inhibitor-induced apoptosis through the generation of reactive oxygen species. *J. Thorac. Cardiovasc. Surg.* **2004**, *128*, 740−748.
(20) Jones, D. R.; Moskaluk, C. A.; Gillenwater, H. H.; Petroni, G. R.; Burks, S. G.; Philips, J.; Rehm, P. K.; Olazagasti, J.; Kozower, B. D.; Bao, Y. Phase I trial of induction histone deacetylase and proteasome inhibition followed by surgery in non-small-cell lung cancer. *J. Thorac. Oncol.* **2012**, *7*, 1683−1690.
(21) Ling, Y. H.; Liebes, L.; Zou, Y.; Perez-Soler, R. Reactive oxygen species generation and mitochondrial dysfunction in the apoptotic response to bortezomib, a novel proteasome inhibitor, in human H460 non-small cell lung cancer cells. *J. Biol. Chem.* **2003**, *278*, 33714−33723.
(22) Saavedra, J. E.; Srinivasan, A.; Bonifant, C. L.; Chu, J.; Shanklin, A. P.; Flippen-Anderson, J. L.; Rice, W. G.; Turpin, J. A.; Davies, K. M.; Keefer, L. K. The secondary amine/nitric oxide complex ion $R_2N[N(O)NO]^-$ as nucleophile and leaving group in S_NAr reactions. *J. Org. Chem.* **2001**, *66*, 3090−3098.
(23) Saavedra, J. E.; Booth, M. N.; Hrabie, J. A.; Davies, K. M.; Keefer, L. K. Piperazine as a linker for incorporating the nitric oxide-releasing diazeniumdiolate group into other biomedically relevant functional molecules. *J. Org. Chem.* **1999**, *64*, 5124−5131.
(24) Romanowska, M.; Maciag, A.; Smith, A. L.; Fields, J. R.; Fornwald, L. W.; Kikawa, K. D.; Kasprzak, K. S.; Anderson, L. M. DNA damage, superoxide, and mutant K-ras in human lung adenocarcinoma cells. *Free Radical Biol. Med.* **2007**, *43*, 1145−1155.
(25) Ji, X.; Pal, A.; Kalathur, R.; Hu, X.; Gu, Y.; Saavedra, J. E.; Buzard, G. S.; Srinivasan, A.; Keefer, L. K.; Singh, S. V. Structure-based design of anticancer prodrug PABA/NO. *Drug Des. Dev. Ther.* **2008**, *2*, 123−130.
(26) Prade, L.; Huber, R.; Manoharan, T. H.; Fahl, W. E.; Reuter, W. Structures of class pi glutathione S-transferase from human placenta in complex with substrate, transition-state analogue and inhibitor. *Structure* **1997**, *5*, 1287−1295.
(27) *MacroModel*, version 9.6; Schrödinger, LLC: New York, NY, 2008.